Up-conversion luminescence polarization control in Er^{3+}-doped $NaYF_4$ nanocrystals*

Hui Zhang(张晖)[1], Yun-Hua Yao(姚云华)[2], Shi-An Zhang(张诗按)[2,†], Chen-Hui Lu(卢晨晖)[3], and Zhen-Rong Sun(孙真荣)[2]

[1] *Institute of Science, Information Engineering University, Zhengzhou* 450001, *China*
[2] *State Key Laboratory of Precision Spectroscopy and Department of Physics, East China Normal University, Shanghai* 200062, *China*
[3] *College of Mechanical Engineering, Shanghai University of Engineering Science, Shanghai* 201620, *China*

(Received 8 August 2015; revised manuscript received 9 October 2015; published online 20 December 2015)

We propose a femtosecond laser polarization modulation scheme to control the up-conversion (UC) luminescence in Er^{3+}-doped $NaYF_4$ nanocrystals dispersed in the silicate glass. We show that the UC luminescence can be suppressed when the laser polarization is changed from linear through elliptical to circular, and the higher repetition rate will yield the lower control efficiency. We theoretically analyze the physical control mechanism of the UC luminescence polarization modulation by considering on- and near-resonant two-photon absorption, energy transfer up-conversion, and excited state absorption, and show that the polarization control mainly comes from the contribution of near-resonant two-photon absorption. Furthermore, we propose a method to improve the polarization control efficiency of UC luminescence in rare-earth ions by applying a two-color femtosecond laser field.

Keywords: up-conversion luminescence, laser polarization, nanocrystal

PACS: 32.80.Qk, 33.80.–b, 61.46.Hk **DOI:** 10.1088/1674-1056/25/2/023201

1. Introduction

Recently, the up-conversion (UC) luminescence of luminescent material doped with rare-earth ions, which converts the low-frequency stimulation into high-frequency emission via two-photon or multi-photon absorption process, has attracted considerable attention because of its unique optical properties, such as narrow emission spectrum, intense luminescence intensity, high conversion efficiency, good optical stability, and long luminescence lifetime, and has been widely used in various related fields, such as light-emitting diodes,[1,2] fiber optic communication,[3,4] laser sources,[5,6] color display,[7,8] medical imaging,[9,10] biological labels,[11,12] etc. If the UC luminescence can be controlled, such as in enhancement, suppression or multi-color tuning, its relevant applications can be greatly extended. By now, several schemes have been proposed to experimentally realize the UC luminescence enhancement, suppression, and tuning. For example, a common method is to adjust the material property by varying its dopant-host combination,[13–15] nanoparticle size,[16,17] and dopant concentration[18,19] in the synthesis process, and the other common method is to control the laser parameter by varying the excitation wavelength,[20] power density,[21] pulse duration,[22] spectral phase[23,24] or polarization.[25,26] In addition, applying an electric or magnetic field has also been proved to be an available method to control the UC luminescence.[27,28]

Because of the surface effect, volume effect, quantum size effect, and macroscopic quantum tunnel effect, the nanocrystal material shows different performances in magnetic, optic, electric, and chemical properties compared with normal bulk material.[29,30] The nanocrystal material doped with rare-earth ions combines the unique optical properties of both nanocrystals and rare-earth ions, and therefore is shown to be a promising alternative to luminescent materials, such as $NaGdF_4$-based nanocrystals for biological fluorescence imaging,[31] $NaYbF_4$:Tm^{3+}/Ho^{3+}/Er^{3+} and $NaYF_4$:Yb^{3+} used as biological markers.[32] In the present work, we experimentally and theoretically show that the UC luminescence in Er^{3+}-doped $NaYF_4$ nanocrystals dispersed in the silicate glass can be controlled by varying the femtosecond laser polarization. Our experimental results show that the UC luminescence intensity can be reduced when the laser polarization is changed from linear through elliptical to circular, but the control efficiency will be affected by the laser repetition rate, and the lower repetition rate will yield the higher control efficiency. Our theoretical studies indicate that the polarization modulation depends on the near-resonant two-photon absorption but is independent of the on-resonant two-photon absorption, energy transfer up-conversion, and excited state absorption. In addition, a two-color femtosecond laser field is proposed to improve the polarization control efficiency of UC luminescence by keeping the near-resonant two-photon absorption process but exclud-

*Project supported by the Young Scientists Fund of the National Natural Science Foundation of China (Grant No. 11304396), the National Natural Science Foundation of China (Grant Nos. 11474096 and 51132004), and the Shanghai Municipal Science and Technology Commission, China (Grant No. 14JC1401500).

†Corresponding author. E-mail: sazhang@phy.ecnu.edu.cn

© 2016 Chinese Physical Society and IOP Publishing Ltd

ing the other excitation processes.

2. Experimental arrangement

Our experimental arrangement is shown in Fig. 1, where a Ti-sapphire mode-locked regenerative amplifier (Spectra-Physics, Spitfire) with a pulse duration of about 50 fs, central wavelength of 800 nm, and repetition rate of 1 kHz and a mode-locked Ti-sapphire laser oscillator (Spectra-Physics, Tsunami) with a pulse duration of about 35 fs, central wavelength of 800 nm, and repetition rate of 80 MHz are used as the excitation sources, and two removable mirrors are utilized to switch the two laser sources. A quarter wave plate (Thorlabs, AQWP05M-980, 690–1120 nm) is used to vary the laser polarization from linear through elliptical to circular. The polarization-modulated femtosecond laser pulse is focused into the experimental sample with a lens of 50-mm focal length, and the laser intensities at the focus area are estimated to be 4×10^{13} W/cm^2 for the 1-kHz laser amplifier and about 2×10^{11} W/cm^2 for the 80-MHz laser oscillator respectively. All luminescence signals emitted from the sample are collected perpendicularly by a telescope system and recorded by a spectrometer with charge-coupled device (CCD).

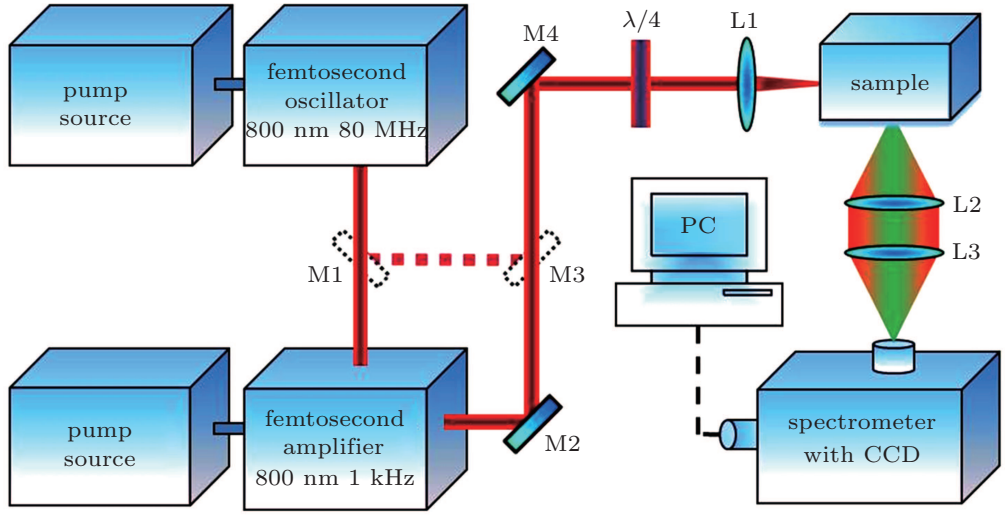


Fig. 1. (color online) Schematic diagram of experimental arrangement for polarization control of UC luminescence in Er^{3+}-doped $NaYF_4$ nanocrystals. Here, M1 and M3 are removable mirrors, which are used to switch the 1-kHz femtosecond laser amplifier and 80-MHz femtosecond laser oscillator.

In our experiment, the glass ceramic containing Er^{3+}-doped $NaYF_4$ nanocrystals is used as our study example, which is synthesized via modification from melt-quenching to subsequent heat treatment. The precursor sample is prepared with the molar ratio of $40SiO_2$-$25Al_2O_3$-$18Na_2CO_3$-$10YF_3$-7NaF-$1ErF_3$. The original material is mixed and melted in a covered platinum crucible at a temperature of 1450 °C for 45 min in the ambient atmosphere and then cast into a brass mold followed by annealing at a temperature of 450 °C for 10 h. The synthesized glass is heated to a temperature of 600 °C in steps of 10 K/min, kept at this temperature for 2 h, and then cooled to room temperature to form the glass ceramic through crystallization. The glass ceramic sample is cut and polished for optical measurement in our experiment. X-ray diffraction (XRD) analysis is performed to identify the crystallization phase with a power diffractometer (Bruker D8 Advance) operated at 40 kV and 40 mA, and the measured result is shown in Fig. 2, where Cu Kα is used as a radiation source, and 2θ is scanned in a range of 20°–90° in steps of 0.01°. Multiple sharp peaks are observed in the XRD curve, which can be attributed to cubic α-$NaYF_4$ crystalline phase, indicating the crystallization of α-$NaYF_4$ during thermal treatment.

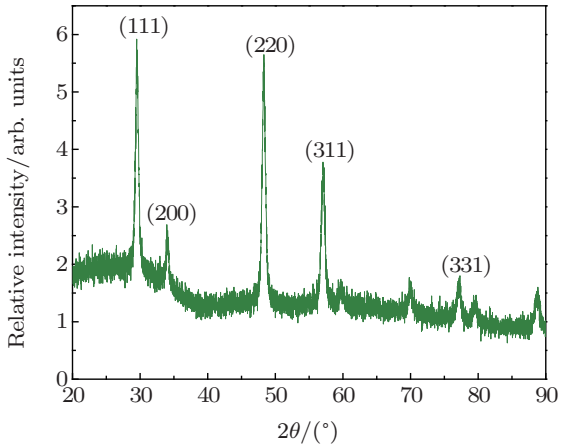


Fig. 2. (color online) XRD curve of glass ceramic containing Er^{3+}-doped $NaYF_4$ nanocrystals. Here, those peaks from α-$NaYF_4$ are indexed.

Transmission electron microscopy (TEM) images of the sample are provided in Fig. 3(a), which show that nanocrystals with an average size of 20 nm–30 nm disperse densely in the glass matrix. Besides, the high-resolution TEM (HRTEM) of an individual α-$NaYF_4$ in Fig. 3(b) displays the lattice fringe

with a distance of 0.3 nm.

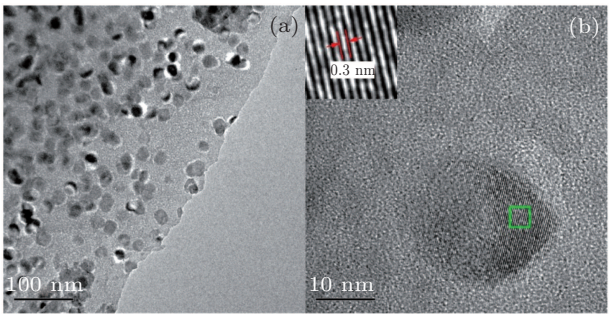


Fig. 3. (color online) The TEM (a) and HRTEM (b) images of the glass ceramic containing Er^{3+}:$NaYF_4$ nanocrystals.

3. Results and discussion

The UV-VIS-NIR absorption spectrum of Er^{3+}-doped $NaYF_4$ nanocrystals is shown in Fig. 4(a). As can be seen, six main absorption peaks appear around the wavelengths of 377, 407, 487, 545, 651, and 799 nm, which can be attributed to the absorptions of these excited states $^4G_{11/2}$, $^2H_{9/2}$, $^4F_{7/2}$, $^4S_{3/2}$, $^4F_{9/2}$, and $^4I_{9/2}$. The measured UC luminescence spectrum in the visible light region is shown in Fig. 4(b). One can see that five luminescence signals are observed around the wavelengths of 408, 475, 527, 547, and 656 nm, which can be attributed to the state transitions from the five excited states $^2H_{9/2}$, $^4F_{7/2}$, $^2H_{11/2}$, $^4S_{3/2}$, and $^4F_{9/2}$ to the ground state $^4I_{15/2}$, respectively. It is easy to observe that the green and red UC luminescence signals dominate the visible light spectrum, and therefore our goal in this work is to control the green and red UC luminescence by varying the femtosecond laser polarization.

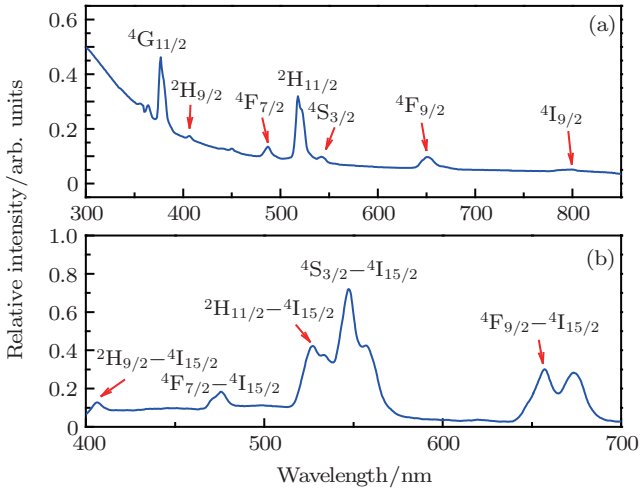


Fig. 4. (color online) The UV-VIS-IR absorption (a) of the glass ceramic containing Er^{3+}:$NaYF_4$ nanocrystals and UC luminescence spectrum (b) of the sample excited by 800-nm femtosecond laser with a repetition rate of 1 kHz.

Figure 5(a) shows the green (546 nm) (green triangles) and red (656 nm) (red circles) UC luminescence intensities each as a function of quarter wave plate angle excited by the 1-kHz laser amplifier. The quarter wave plate angle has no effect on the intensity of the laser past the $\lambda/4$ plate, which is confirmed experimentally. As can be seen, both the green and red UC luminescence intensities can be controlled by the laser polarization modulation, which decreases when the laser polarization changes from linear through elliptical to circular. But their control efficiencies are different, which are, respectively, 13% and 6%, and the green UC luminescence obtains the higher control efficiency. Here, the control efficiency is defined as $\eta = 1 - I^{\min}/I^{\max}$, where $I^{\max}$ and $I^{\min}$ represent the maximum and minimum luminescence intensities (in units of a.u., i.e., atomic unit), respectively. However, when the excitation source is switched to the 80-MHz laser oscillator, as shown in Fig. 5(b), both the green and red UC luminescence intensities almost remain constant, that is to say, the green and red luminescence are independent of the laser polarization. Obviously, the laser repetition rate will affect the polarization control efficiency of UC luminescence intensity, and a higher repetition rate will yield a lower control efficiency. Therefore, to obtain the effective polarization control of the green and red UC luminescence in the Er^{3+}-doped $NaYF_4$ nanocrystals, it is critical to utilize the low laser repetition rate, such as 1 kHz.

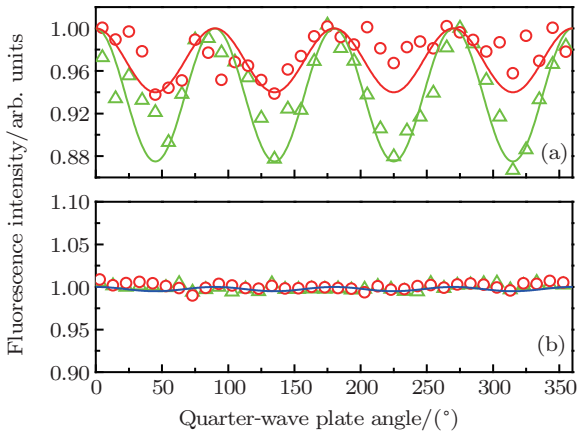


Fig. 5. (color online) Variations of experimental green (546 nm) (green triangles) and red (656 nm) (red circles) up-conversion luminescence intensities with $\lambda/4$ wave plate angle with using a 1-kHz laser amplifier (a) and an 80-MHz laser oscillator (b), together with the theoretical simulations (solid lines).

According to the absorption and luminescence spectra of Er^{3+}-doped $NaYF_4$ nanocrystals in Fig. 4, we present the excitation and detection scheme in our experiment as shown in Fig. 6. The population in the ground state $^4I_{15/2}$ is pumped to the excited state $^2H_{9/2}$ through a resonance-mediated two-photon absorption (TPA) process, which contains on- and near-resonant two-photon absorption. The on-resonant two-photon absorption means that the population in the ground state $^4I_{15/2}$ is pumped to the intermediate state $^4I_{9/2}$ by absorbing one photon and then is further pumped to the excited state $^2H_{9/2}$ by absorbing another photon, whereas the near-resonant two-photon absorption means that the population in the ground state $^4I_{15/2}$ is directly pumped to the excited state

$^2H_{9/2}$ by simultaneously absorbing two photons without passing through the intermediate state $^4I_{9/2}$. The population in the excited state $^2H_{9/2}$ can spontaneously decay to the ground state $^4I_{15/2}$ through these lower excited states $^2H_{11/2}$, $^4S_{3/2}$, and $^4F_{9/2}$, and emits the green and red up-conversion luminescence. The population in the intermediate state $^4I_{9/2}$ by single photon absorption (SPA) process can also relax to the two lower excited states $^4I_{11/2}$ and $^4I_{13/2}$, and then is further pumped to the higher excited states $^4F_{7/2}$ and $^4F_{9/2}$ by energy transfer up-conversion (ETU) process due to the higher dopant concentration. Generally, the excited state lifetime of rare-earth ions is relatively long in the range of microseconds. If the time separation between the laser pulses is shorter than the excited state lifetime, the populations in the excited states $^4I_{9/2}$, $^4I_{11/2}$, and $^4I_{13/2}$ can be further pumped to these higher excited states $^2H_{9/2}$, $^4F_{3/2}$, and $^4S_{3/2}$ by absorbing the photons from subsequent laser pulses (see Fig. 6(b)), which is called excited state absorption (ESA) process, and also emits green and red UC luminescences.

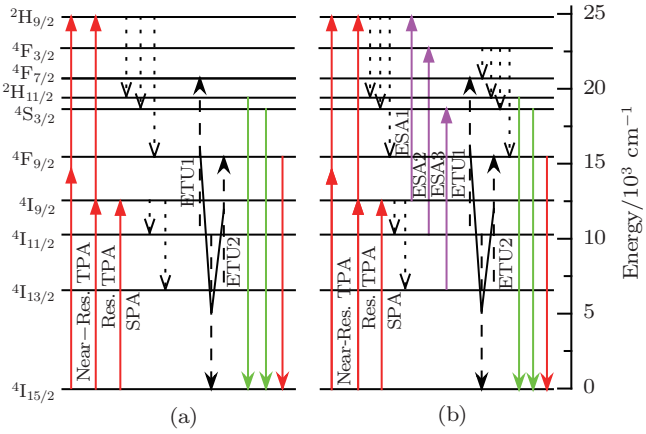


Fig. 6. (color online) Energy levels of Er^{3+} ions and possible pathways of green and red UC luminescences generated by a 1-kHz laser amplifier (a) and an 80-MHz laser oscillator (b).

As can be seen in Fig. 6, the green or red UC luminescence produced by the on-resonant TPA, ETU, and ESA processes depends on the population in the intermediate state $^4I_{9/2}$, and thus their intensities cannot be controlled by varying the laser polarization since the absorption in the intermediate state $^4I_{9/2}$ is a single photon process, which is independent of the laser polarization. Consequently, the polarization modulations of green and red UC luminescence should result from the near-resonant TPA process. Thus, the experimental observation in Fig. 5 can be well explained. In the case of the low repetition rate of 1 kHz, corresponding to the laser pulse separation of 1 ms, only one laser pulse arrives within the lifetime of the excited state since the excited state lifetime is far smaller than the laser pulse separation (see Fig. 6(a)). Compared with the green UC luminescence, the red UC luminescence generation additionally contains the ETU2 process, which will suppress the polarization control efficiency of red UC luminescence, and therefore the polarization control efficiency of red UC luminescence is lower than that of green UC luminescence (see Fig. 5(a)). However, for the case of the high repetition rate of 80 MHz, corresponding to the laser pulse separation of 12.5 ns, multiple laser pulses arrive within the lifetime of the excited state because the excited state lifetime is far longer than the laser pulse separation (see Fig. 6(b)). The green and red UC luminescence contain the contribution of the ESA process, and thus their polarization control efficiencies will be greatly suppressed since the ESA process is independent of the laser polarization (see Fig. 5(b)).

As discussed above, the polarization modulations of green and red UC luminescence come from the contribution of the near-resonant TPA process. In order to demonstrate the effect of the femtosecond laser polarization on the near-resonant TPA process, we theoretically simulate the resonance-mediated TPA in the Er^{3+} ions by a time-dependent perturbation theory.[33] Usually, the multi-photon absorption in a quantum system with a broad absorption line can be simplified into the sum of all individual transitions. Based on the theoretical model of the atom system with narrow absorption line limit,[34,35] the resonance-mediated two-photon transition probability $S^{(1+1)}$ in the Er^{3+} ions can be approximated as

$$S^{(1+1)} \propto \int_{-\infty}^{+\infty} \mathrm{d}\omega_f A(\omega_f) \left| \int_{-\infty}^{+\infty} A(\omega_i) \times \int_{-\infty}^{+\infty} E(t_1) \exp\left[\mathrm{i}(\omega_f - \omega_i) t_1\right] \times \int_{-\infty}^{t_1} E(t_2) \exp(\mathrm{i}\omega_i t_2)\, \mathrm{d}t_2\, \mathrm{d}t_1\, \mathrm{d}\omega_i \right|^2, \quad (1)$$

where ω_i and ω_f are the resonant frequencies of intermediate state $|i\rangle$ (i.e., $^4I_{9/2}$) and final excited state $|f\rangle$ (i.e., $^2H_{9/2}$), and $A(\omega_i)$ and $A(\omega_f)$ are the absorption line-shape functions of intermediate state $|i\rangle$ and final excited state $|f\rangle$. By transforming Eq. (1) into the frequency domain, the transition probability $S^{(1+1)}$ can be rewritten as

$$S^{(1+1)} \propto \int_{-\infty}^{+\infty} \mathrm{d}\omega_f A(\omega_f) \left| P^{(1+1)}_{\mathrm{On-Res.}} + P^{(1+1)}_{\mathrm{Near-Res.}} \right|^2, \quad (2)$$

with

$$P^{(1+1)}_{\mathrm{On-Res.}} = \mathrm{i}\pi \int_{-\infty}^{+\infty} \mathrm{d}\omega_i A(\omega_i) E(\omega_f - \omega_i) E(\omega_i), \quad (3)$$

and

$$P^{(1+1)}_{\mathrm{Near-Res.}} = \wp \int_{-\infty}^{+\infty} \mathrm{d}\omega E(\omega_f - \omega) E(\omega)/(\omega_i - \omega), \quad (4)$$

where $P^{(1+1)}_{\mathrm{On-Res.}}$ and $P^{(1+1)}_{\mathrm{Near-Res.}}$ are, respectively, the on- and near-resonant two-photon transition amplitudes, $E(\omega) = E_0(\omega)\exp[\mathrm{i}\Phi(\omega)]$ is the Fourier transform of $E(t)$, and $E_0(\omega)$ and $\Phi(\omega)$ are the spectral amplitude and phase respectively. As can be seen from Eq. (2), the resonance-mediated TPA process can be decomposed into on- and near-resonant components $P^{(1+1)}_{\mathrm{On-Res.}}$ and $P^{(1+1)}_{\mathrm{Near-Res.}}$. The on-resonant component

$P^{(1+1)}_{\mathrm{On-Res.}}$ involves all on-resonant two-photon excitation pathways with the frequencies of ω_i and ω_f–ω_i, whereas the near-resonant component $P^{(1+1)}_{\mathrm{Near-Res.}}$ involves all other near-resonant two-photon excitation pathways with the frequencies of ω and ω_f–ω. The on-resonant component is excluded from the near-resonant component by Cauchy's principal value operator $\wp$. Obviously, the laser spectral width or pulse width will affect both the on- and near-resonant components, but the effect is greater for the near-resonant component since more photon pairs are absorbed by the near-resonant two-photon excitation process under the femtosecond laser field. For the transform-limited femtosecond laser pulse (i.e., $\Phi(\omega)=0$), the value of laser field $E(\omega)$ is a positive real number for any laser frequency, and thus the value of on-resonant component $P^{(1+1)}_{\mathrm{On-Res.}}$ is an imaginary number while the value of near-resonant component $P^{(1+1)}_{\mathrm{Near-Res.}}$ is a real number. In this case, the transition probability $S^{(1+1)}$ can be further simplified into

$$S^{(1+1)} \propto S^{(1+1)}_{\mathrm{On-Res.}} + S^{(1+1)}_{\mathrm{Near-Res.}}, \tag{5}$$

with

$$S^{(1+1)}_{\mathrm{On-Res.}} = \int_{-\infty}^{+\infty} \mathrm{d}\,\omega_f A\left(\omega_f\right) \left|P^{(1+1)}_{\mathrm{On-Res.}}\right|^2, \tag{6}$$

and

$$S^{(1+1)}_{\mathrm{Near-Res.}} = \int_{-\infty}^{+\infty} \mathrm{d}\,\omega_f A\left(\omega_f\right) \left|P^{(1+1)}_{\mathrm{Near-Res.}}\right|^2. \tag{7}$$

When a linearly polarized laser field is modulated by the quarter wave plate, its polarization status will be changed. Mathematically, the polarization-modulated laser field can be defined by the function of

$$\boldsymbol{E}_{\lambda/4}(t) = \cos(\theta)\, E(t)\, \boldsymbol{e}_x + \sin(\theta)\, E(t)\, \boldsymbol{e}_y, \tag{8}$$

where $\boldsymbol{e}_x$ and $\boldsymbol{e}_y$ represent the polarization directions in a rectangular coordinate system, and θ is the angle between the input laser polarization direction and the optical axis of the quarter wave plate. It is easy to verify that the output laser fields are linear polarization for $\theta = m\pi/2$ ($m = 0,1,2,\ldots$), circular polarization for $\theta = (2m+1)\pi/4$ and elliptical polarization for other angle θ, respectively. The two photons via on-resonant absorption can come from the same polarization direction (i.e., $\boldsymbol{e}_x\boldsymbol{e}_x$ and $\boldsymbol{e}_y\boldsymbol{e}_y$) or different polarization directions (i.e., $\boldsymbol{e}_x\boldsymbol{e}_y$ and $\boldsymbol{e}_y\boldsymbol{e}_x$), whereas the two absorbed photons via near-resonant absorption can only come from the same polarization direction (i.e., $\boldsymbol{e}_x\boldsymbol{e}_x$ and $\boldsymbol{e}_y\boldsymbol{e}_y$).[36] Thus, the on-resonant term $S^{(1+1)}_{\mathrm{On-Res.}}$ and near-resonant term $S^{(1+1)}_{\mathrm{Near-Res.}}$ induced by the polarization-modulated laser field can be written as

$$\begin{aligned} S^{(1+1)}_{\mathrm{On-Res.}} &= \left[\cos^4(\theta) + \sin^4(\theta) + 2\cos^2(\theta)\sin^2(\theta)\right] \\ &\quad \times \int_{-\infty}^{+\infty} \mathrm{d}\,\omega_f A\left(\omega_f\right) \left|P^{(1+1)}_{\mathrm{On-Res.}}\right|^2 \\ &= \int_{-\infty}^{+\infty} \mathrm{d}\,\omega_f A\left(\omega_f\right) \left|P^{(1+1)}_{\mathrm{On-Res.}}\right|^2, \end{aligned} \tag{9}$$

and

$$\begin{aligned} S^{(1+1)}_{\mathrm{Near-Res.}} &= \left[\cos^4(\theta) + \sin^4(\theta)\right] \\ &\quad \times \int_{-\infty}^{+\infty} \mathrm{d}\,\omega_f A\left(\omega_f\right) \left|P^{(1+1)}_{\mathrm{Near-Res.}}\right|^2. \end{aligned} \tag{10}$$

As can be seen from Eqs. (9) and (10), the on-resonant term $S^{(1+1)}_{\mathrm{On-Res.}}$ is independent of the laser polarization, whereas the near-resonant term $S^{(1+1)}_{\mathrm{Near-Res.}}$ is related to the laser polarization (i.e., θ), which is consistent with the above discussion. One can see that $S^{(1+1)}$ is a maximal value for $\theta = m\pi/2$ (linear polarization) and a minimal value for $\theta = (2m+1)\pi/4$ (circular polarization). Therefore, when the laser polarization is changed from linear through elliptical to circular, the transition probability $S^{(1+1)}$ decreases. Obviously, the theoretical result is in good agreement with the experimental observation. In Fig. 5, we also show the theoretical simulation, and here the weight of the near-resonant two-photon absorption in the whole excitation process is taken into account.

Since the polarization modulations of green and red UC luminescence result from the near-resonant TPA process, it is necessary to increase the weight of the near-resonant TPA component in the whole excitation process in order to improve the polarization control efficiency. One simple way is to keep the near-resonant TPA process and exclude other excitation processes. In this experiment, the on-resonant TPA, ESA and ETU processes are correlated with the absorption in the intermediate state $^4\mathrm{I}_{9/2}$, and thus a two-color laser field may be a well-established tool to eliminate these excitation processes but keep the near-resonant TPA process. In the two-color excitation process, both laser fields should be far from the resonant absorption of intermediate state $^4\mathrm{I}_{9/2}$, but the sum of their frequencies should be equal to the transition frequency of excited state $^2\mathrm{H}_{9/2}$. By such a two-color laser field excitation, the green and red UC luminescence may be suppressed, but their polarization control efficiencies should be improved, and the polarization modulation should not be affected by the laser repetition rate.

4. Conclusions

In this study, we experimentally and theoretically demonstrate that the femtosecond laser polarization can control the UC luminescence in Er^{3+}-doped $NaYF_4$ nanocrystals dispersed in the silicate glass. It is shown that the circular polarization will suppress the UC luminescence, but the polarization control is affected by the laser repetition rate, and a higher repetition rate leads to a lower control efficiency. It is also shown that the UC luminescences come from the TPA, ETU, and ESA processes, but the polarization modulation only results from the near-resonant TPA process. Furthermore, the two-color femtosecond laser field is shown to be

a feasible method to keep the near-resonant TPA process and exclude other excitation processes, and consequently can improve the polarization control efficiency. The study presents a clear physical process for the polarization control of UC luminescence in Er^{3+}-doped $NaYF_4$ nanocrystals, which is very useful for further understanding and controlling the UC luminescences in various luminescent materials. The laser polarization modulation provides a very simple method to control various nonlinear optical processes, and therefore these theoretical and experimental results can be used as the study basis in related fields.

References

[1] Sivakumar S, van Veggel F C M and Raudsepp M 2005 *J. Am. Chem. Soc.* **127** 12464
[2] Kido J, Hayase H, Hongawa K, Nagai K and Okuyama K 1994 *Appl. Phys. Lett.* **65** 2124
[3] Tessler N, Medvedev V, Kazes M, Kan S and Banin U 2002 *Science* **295** 1506
[4] Zhou P, Wang X, Ma Y, Lü H and Liu Z J 2012 *Laser Phys.* **22** 1744
[5] Scheps R 1996 *Prog. Quantum Electron.* **20** 271
[6] Wintner E, Sorokin E and Sorokina I T 2011 *Laser Phys.* **11** 1193
[7] Downing E, Hesselink L, Ralston J and Macfarlane R 1996 *Science* **273** 1185
[8] Glaspell G, Anderson J, Wilkins J R and El-Shall M S 2008 *J. Phys. Chem. C* **112** 11527
[9] Suyver J F, Aebischer A, Biner D, Gerner P, Grimm J, Heer S, Krämer K W, Reinhard C and Güdel H U 2005 *Opt. Mater.* **27** 1111
[10] Haase M and Schäfer H 2011 *Angew. Chem. Int. Ed.* **50** 5808
[11] Wang F, Tan W B, Zhang Y, Fan X and Wang M 2006 *Nanotechnology* **17** R1
[12] Wolska E, Kaszewski J, Kiełbik P, Grzyb J, Godlewski M M and Godlewski M 2014 *Opt. Mater.* **36** 1655
[13] Heer S, Kömpe K, Güdel H U and Haase M 2004 *Adv. Mater.* **16** 2102
[14] Ehlert O, Thomann R, Darbandi M and Nann T 2008 *ACS Nano* **2** 120
[15] Dai L, Xu C, Zhang Y, Li D Y and Xu Y H 2013 *Chin. Phys. B* **22** 094201
[16] Mai H X, Zhang Y W, Sun L D and Yan C H 2007 *J. Phys. Chem. C* **111** 13721
[17] Bai X, Song H W, Pan G H, Lei Y Q, Wang T, Ren X G, Lu S Z, Dong B, Dai Q L and Fan L B 2007 *J. Phys. Chem. C* **111** 13611
[18] Wang F and Liu X G 2008 *J. Am. Chem. Soc.* **130** 5642
[19] Wang L, Yan R, Huo Z, Wang L, Zeng J, Bao J, Wang X, Peng Q and Li Y 2005 *Angew. Chem. Int. Ed.* **44** 6054
[20] Franzò G, Iacona F, Vinciguerra V and Priolo F 2000 *Mater. Sci. Eng. B* **69** 335
[21] Bednarkiewicz A, Wawrzynczyk D, Nyk M and Samoć M 2011 *J. Rare Earths* **29** 1152
[22] Gainer C F, Joshua G S, De Silva C R and Romanowski M 2011 *J. Mater. Chem.* **21** 18530
[23] Zhang S A, Lu C H, Jia T Q, Qiu J R and Sun Z R 2013 *Appl. Phys. Lett.* **103** 194104
[24] Zhang S A, Xu S W, Ding J X, Lu C H, Jia T Q, Qiu J R and Sun Z R 2014 *Appl. Phys. Lett.* **104** 014101
[25] Zhou J J, Chen G X, Wu E, Bi G, Wu B T, Teng Y, Zhou S F and Qiu J R 2013 *Nano Lett.* **13** 2241
[26] Lu C H, Zhang H, Zhang S A and Sun Z R 2012 *Chin. Phys. B* **21** 123202
[27] Hao J H, Zhang Y and Wei X H 2011 *Angew. Chem. Int. Ed.* **50** 6876
[28] Liu Y X, Wang D S, Shi J X, Peng Q and Li Y D 2013 *Angew. Chem. Int. Ed.* **52** 4366
[29] Mai H X, Zhang Y W, Si R, Yan Z G, Sun L D, You L P and Yan C H 2006 *J. Am. Chem. Soc.* **128** 6426
[30] Alivisatos A P 1996 *J. Phys. Chem.* **100** 13226
[31] Zhou J J, Shirahata N, Sun H T, Ghosh B, Ogawara M, Teng Y, Zhou S F, Chu R G S, Fujii M and Qiu J R 2013 *J. Phys. Chem. Lett.* **4** 402
[32] Ehlert O, Thomann R, Darbandi M and Nann T 2008 *ACS Nano* **2** 120
[33] Meshulach D and Silberberg Y 1999 *Phys. Rev. A* **60** 1287
[34] Dudovich N, Dayan B, Faeder S M G and Silberberg Y 2001 *Phys. Rev. Lett.* **86** 47
[35] Dayan B, Pe'Er A, Friesem A A and Silberberg Y 2004 *Phys. Rev. Lett.* **93** 23005
[36] Xu S W, Huang Y X, Yao Y H, Jia T Q, Ding J X, Zhang S A and Sun Z R 2015 *J. Phys. B: At. Mol. Opt. Phys.* **48** 135402